# Density Functional Theory Calculations of Nitrogen Hyperfine and Quadrupole Coupling Constants in Oxovanadium(IV) Complexes

**Alexander C. Saladino and Sarah C. Larsen***

*Department of Chemistry, University of Iowa, Iowa City, Iowa 52242*

*Received: January 14, 2003; In Final Form: March 21, 2003*

Relativistic density functional theory (DFT) calculations of nitrogen hyperfine and quadrupole coupling constants were conducted for a series of oxovanadium complexes with axial and equatorial nitrogen ligands. The computational results qualitatively reproduced the observed experimental trends in nitrogen hyperfine coupling constants with ligand type (amine, imine, and isothiocyanate) and coordination (axial vs equatorial). The best quantitative agreement between calculated and experimental nitrogen coupling constants was obtained using the scalar-relativistic, spin-unrestricted, open-shell Kohn−Sham (SR UKS) method. These results have important implications for the interpretation of high-resolution electron paramagnetic resonance (EPR) spectra of oxovanadium complexes with nitrogen ligands.

## Introduction

Experimental electron spin−echo envelope modulation (ESEEM) and electron nuclear double resonance (ENDOR) measurements of $VO^{2+}$ ligand hyperfine and quadrupole coupling constants have provided valuable information about local active site structure in many different biological systems.[1−10] Model complex studies have been used to guide the interpretation of the experimental data. For example, experimental ESEEM studies of model $VO^{2+}$ complexes containing imidazole and amine ligands have been used to assign spectroscopic features in $VO^{2+}$ metalloenzymes to coordinated histidine[1−10] or lysine residues.[11,12] The measured values for isotropic and anisotropic nitrogen hyperfine coupling constants have been used to develop models of the active site structure in biological systems containing $VO^{2+}$ centers.

The nitrogen nuclear quadrupole coupling constant (NQCC) is the coupling between the nuclear quadrupole moment of the nitrogen ($^{14}N$, $I = 1$) nucleus and the electric field gradient (EFG) at the nucleus due to a nonspherical charge distribution.[13−18] Nuclear quadrupole coupling constants (NQCC) for nitrogen are sensitive to the electronic environment of the nitrogen nucleus. NQCCs can be measured experimentally in the gas phase by microwave spectroscopy and in the solid phase by nuclear quadrupole resonance (NQR) spectroscopy. Experimental nitrogen NQCCs can also be measured using ESEEM spectroscopy.[19−23]

Recently, Kamada and co-workers[24] measured the nitrogen hyperfine and quadrupole coupling constants for a group of oxovanadium amine, imine, and isothiocyanate complexes using ESEEM spectroscopy. Reijerse and co-workers[19] have also measured the nitrogen hyperfine and quadrupole coupling constants for several oxovanadium model complexes. Lobrutto et al.[6] have measured the ESEEM spectra for several oxovanadium model complexes with axial nitrogen ligands so that axial versus equatorial ligation could be distinguished in vanadoprotein systems. In the studies mentioned above, the objective has been to develop a body of model compound ESEEM data so that the ESEEM data for biological systems containing $VO^{2+}$ centers could be interpreted. In these systems, ESEEM spectroscopy is often used to determine the identity and coordination of ligands near the $VO^{2+}$ center.

The interpretation of experimental ESEEM and ENDOR data for biological $VO^{2+}$ systems could be further enhanced by density functional theory (DFT) calculations of ligand hyperfine and quadrupole tensors. With the insight provided by DFT calculations, more detailed structural information could potentially be obtained from high-resolution EPR data. However, few computational studies have been published in which ligand hyperfine coupling constants for transition metal complexes have been reported.[25−30] One concern is that because the spin densities on the ligands in which the unpaired electron is localized in a metal singly occupied molecular orbital (SOMO) are very small, 1−2 orders of magnitude smaller than transition metal hyperfine coupling constants, the computational methods may show significant quantitative deviations from experimental values.[25]

To assess the accuracy of the DFT calculations of the nitrogen-ligand coupling constants for vanadyl complexes and to enable the structural interpretation of high-resolution EPR data, DFT calculations were completed for a group of model complexes for which experimental EPR data and, in most cases, crystal structures were available. These model complexes will serve as a testing ground for the application of DFT methods to the calculation of ligand hyperfine and quadrupole coupling constants. In this study, the nitrogen hyperfine and quadrupole coupling constants for a group of $VO^{2+}$ complexes (Figure 1) containing amine, imine, and isothiocyanate groups were calculated using relativistic DFT calculations. The results were compared with experimental data obtained from ESEEM measurements.

## Theoretical Details

**Geometry Optimization.** Calculations of the nitrogen hyperfine coupling constants for $VO^{2+}$ complexes with equatorial nitrogen ligands were performed using the molecular structures from the X-ray diffraction (XRD) data for VO(edda),[31] $VO(meox)_2$,[32] VO(salen),[33] and $[VO(SCN)_4]^{2-}$,[34] where $H_2$edda = ethylenediamine-*N*,*N*′-diacetic acid, meox = oxobis(2-me-

* To whom correspondence should be addressed. Fax: 319-335-1270. E-mail: sarah-larsen@uiowa.edu.

10.1021/jp030051t CCC: $25.00 
Published on Web 05/16/2003

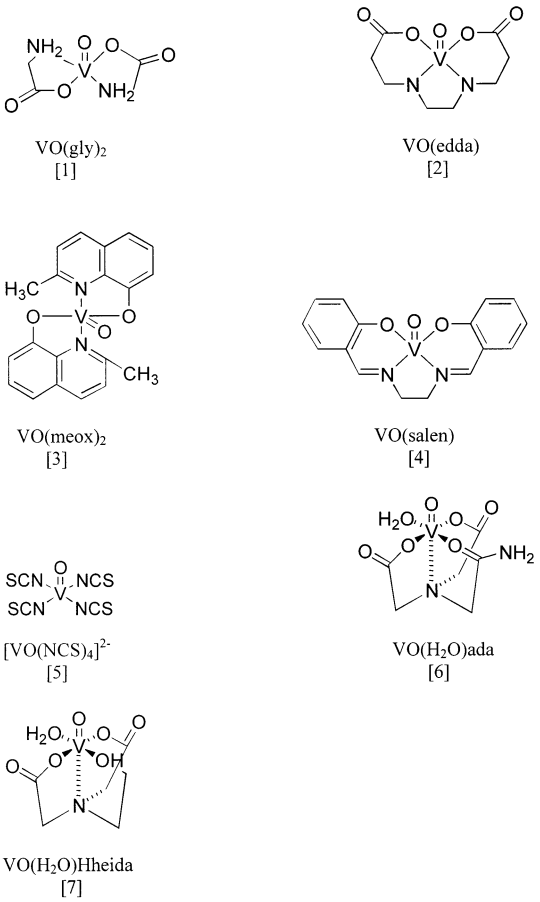


**Figure 1.** Vanadyl complexes with coordinated nitrogen studied: $VO(gly)_2$ [**1**], VO(edda) [**2**], $VO(meox)_2$ [**3**], VO(salen) [**4**], $[VO(SCN)_4]^{2-}$ [**5**], $[VO(H_2O)ada]$ [**6**], and $[VO(H_2O)Hheida]$ [**7**].

thylquinolim-8-olato), and $H_2$salen = *N*,*N*′-bis(salicylidene)ethylenediamine. The crystal structure was not available for $VO(gly)_2$, where gly = glycinate, thus the structure was geometry-optimized using the B3PW91[35,36] density functional and the TZV[37,38] basis set with Gaussian 98.[39] A frequency calculation was performed to ensure that the geometry was at a minimum on the potential energy surface. Calculations of the nitrogen hyperfine coupling constant for $VO^{2+}$ complexes with axially coordinated nitrogen ligands were performed using the molecular structures from the X-ray diffraction (XRD) data for $VO(H_2O)ada$[6] and $VO(H_2O)Hheida$[6] where $H_2ada$ = *N*-(2-acetamido)iminodiacetic acid and $H_3heida$ = *N*-(2-hydroxyethyl)iminodiacetic acid.

**Relativistic Calculations of EPR Parameters with ADF.** The Amsterdam Density Functional program package (ADF 2002.01)[40−42] was used to calculate the EPR parameters for the $VO^{2+}$ model complexes with coordinated nitrogen ligands. The methods for calculating the hyperfine and quadrupole coupling constants were developed by van Lenthe et al.[26,43,44] and are implemented in ADF software. Relativistic effects are included using the zero-order regular approximation (ZORA) Hamiltonian,[45−49] which includes scalar relativistic (SR) and spin−orbit (SO) coupling. Two approaches can be used for *A* tensor calculations with ADF: the scalar-relativistic, spin-unrestricted, open-shell Kohn−Sham (SR UKS) calculation and the spin−orbit coupling and scalar-relativistic, spin-restricted, open-shell Kohn−Sham (SO + SR ROKS) calculation. In the SR UKS method, spin−orbit coupling is not included but spin polarization effects are included. In the SO + SR ROKS method, spin−orbit coupling effects are included but not spin polarization effects. Scalar-relativistic, spin-restricted, open-shell Kohn−Sham (SR ROKS) calculations in which both spin−orbit coupling and spin polarization effects are neglected were used to assess the size of the spin−orbit coupling contributions to the hyperfine tensor. The BP86 density functional was used in the *A* tensor calculations because some results in the literature suggest that the BP86 functional yields the best magnetic resonance parameters compared to the other pure GGA functionals.[50] BP86 uses the parametrized electron gas data given by Vosko et al. for the LDA[51] with the correlation correction by Perdew.[35] The basis set TZ2P was used for all calculations and all atoms. The basis set TZ2P is a double-ζ Slater-type orbital (STO) in the core with a triple-ζ valence shell with two polarizable functions.[52−55]

## Results and Discussion

**DFT Calculations of the Nitrogen Hyperfine Coupling Constants for $VO^{2+}$ Model Complexes with Equatorial Amine, Imine, and Isothiocyanate Ligands.** The nitrogen hyperfine and quadrupole coupling constants were calculated for $VO(gly)_2$, VO(edda), $VO(meox)_2$, VO(salen), and $[VO(SCN)_4]^{2-}$ using the relativistic methods of van Lenthe.[44] The results of three different methods, SR UKS, SO + SR ROKS, and SR ROKS all with the BP86 functional are listed in Table 1. Calculations were completed with the three different methods so that the separate contributions to the nitrogen hyperfine coupling constant from spin polarization and spin−orbit coupling could be determined.

The principal values of the *A* tensor, $A_{11}$, $A_{22}$, and $A_{33}$, are separated into an isotropic component ($A_{iso}$) and the anisotropic or dipolar contribution, $A_{D,x}$, $A_{D,y}$, $A_{D,z}$, such that

$$A_{D,x} = A_{11} - A_{iso}$$

$$A_{D,y} = A_{22} - A_{iso}$$

$$A_{D,z} = A_{33} - A_{iso}$$

where *A* is the hyperfine coupling constant matrix and $A_{11}$, $A_{22}$, and $A_{33}$ are the principal values of *A*. For most of the complexes examined in this study, $A_{33}$ is along (or approximately along) the V−N bond and this is defined to be the *z*-axis for the nitrogen hyperfine interaction.

The experimental and calculated (SR UKS, BP86) $A_{iso}$ values for each of the vanadyl complexes are compared using the bar graph shown in Figure 2. The solid bars represent the SR UKS (ADF, BP86) results, and the dotted bars represent the experimental values. The agreement between the experimental and the calculated $A_{iso}$ values is very good and deviations range from <1% for VO(edda) to ∼10% for $VO(meox)_2$ with an average deviation of ∼4%. The calculated nitrogen $A_{iso}$ values vary systematically with nitrogen type from approximately −5 MHz for amine complexes, to −6 to −7 MHz for imine complexes to −7 to −8 MHz for isothiocyanate complexes. Experimentally, Fukui and co-workers and LoBrutto and co-workers observed a similar dependence of the nitrogen hyperfine coupling constant on the functional group.[6,24]

Both direct singly occupied molecular orbital (SOMO) and indirect spin polarization may contribute to the isotropic hyperfine coupling constant. For these vanadyl complexes, the unpaired electron on the vanadium atom occupies a $d_{xy}$ orbital. Consequently, the overlap with the nitrogen ligand p orbitals is small, and therefore direct spin polarization contributions are not expected to be significant. The primary contribution to the nitrogen isotropic hyperfine coupling constant is from an indirect

**TABLE 1: Calculated (SR UKS, BP86) and Experimental Nitrogen Hyperfine and Quadrupole Coupling Constants for $VO^{2+}$ Complexes with Equatorially Coordinated Ligands[a]**

| | $A_{iso}$ | $A_{D,x}$ | $A_{D,y}$ | $A_{D,z}$ | $Q_{11}$ | $Q_{22}$ | $Q_{33}$ | $\eta$ |
|---|---|---|---|---|---|---|---|---|
| | | | Amine $VO(gly)_2$ | | | | | |
| SR UKS | −4.87 | −0.22 | 0.08 | 0.14 | −1.68 | 1.07 | 0.61 | 0.27 |
| SO + SR ROKS | 0.02 | −0.60 | −0.42 | 1.02 | −1.68 | 1.06 | 0.62 | 0.26 |
| SR ROKS | 0.01 | −0.64 | −0.40 | 1.04 | −1.68 | 1.06 | 0.62 | 0.26 |
| expt[b] | −5.10 | −0.30 | −0.10 | 0.40 | −1.35 | 1.00 | 0.35 | 0.48 |
| | | | VO(edda) | | | | | |
| SR UKS | −4.97 | −0.16 | −0.07 | 0.23 | −1.62 | 1.16 | 0.47 | 0.42 |
| SO + SR ROKS | 0.22 | −0.47 | −0.67 | 1.13 | −1.62 | 1.15 | 0.48 | 0.41 |
| SR ROKS | 0.21 | −0.45 | −0.72 | 1.17 | −1.62 | 1.15 | 0.48 | 0.41 |
| expt[b] | −4.98 | −0.12 | −0.12 | 0.23 | −1.55 | 1.15 | 0.40 | 0.48 |
| | | | Imine $VO(meox)_2$ | | | | | |
| SR UKS | −6.73 | −0.50 | −0.02 | 0.52 | −1.33 | 0.72 | 0.61 | 0.09 |
| SO + SR ROKS | 0.00 | −0.61 | −0.18 | 0.79 | −1.27 | 0.73 | 0.54 | 0.15 |
| SR ROKS | 0.01 | −0.59 | −0.22 | 0.81 | −1.27 | 0.73 | 0.54 | 0.15 |
| expt[c] | −6.18 | −0.57 | 0.06 | 0.51 | −1.17 | 0.66 | 0.51 | 0.13 |
| | | | VO(salen) | | | | | |
| SR UKS (N1) | −6.06 | −0.42 | −0.03 | 0.45 | −1.30 | 0.96 | 0.35 | 0.47 |
| SO + SR ROKS (N1) | 0.03 | −0.92 | 0.29 | 0.63 | −1.19 | 0.94 | 0.25 | 0.58 |
| SR ROKS (N1) | 0.03 | −0.91 | 0.31 | 0.61 | −1.19 | 0.94 | 0.25 | 0.58 |
| SR UKS (N2) | −6.19 | −0.35 | −0.26 | 0.62 | −1.24 | 1.01 | 0.24 | 0.62 |
| SO + SR ROKS (N2) | 0.08 | −1.70 | −0.48 | 2.19 | −1.10 | 1.02 | 0.08 | 0.85 |
| SR ROKS (N2) | 0.10 | −1.66 | −0.46 | 2.12 | −1.10 | 1.02 | 0.08 | 0.85 |
| expt[b] | −5.83 | −0.47 | −0.07 | 0.53 | −1.20 | 0.80 | 0.40 | 0.33 |
| | | | NCS $VO(NCS)_4^{2-}$ | | | | | |
| SR UKS | −7.09 | −0.73 | −0.48 | 1.21 | −0.65 | 0.33 | 0.31 | 0.03 |
| SO + SR ROKS | 0.06 | −0.81 | −0.04 | 0.85 | −0.68 | 0.37 | 0.32 | 0.07 |
| SR ROKS | 0.03 | −0.87 | 0.01 | 0.87 | −0.68 | 0.37 | 0.32 | 0.07 |
| expt[b] | −7.47 | −0.43 | −0.43 | 0.87 | −0.50 | 0.25 | 0.25 | 0.00 |

[a] All values in MHz. [b] Reference 24. [c] Reference 19.

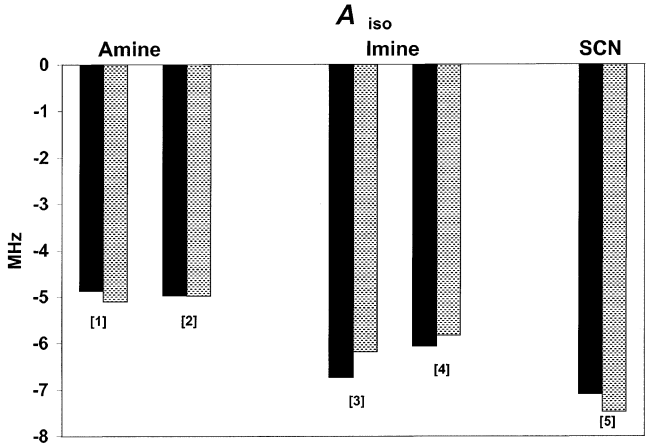


**Figure 2.** The nitrogen isotropic coupling constant ($A_{iso}$) in MHz for $VO(gly)_2$ [**1**], VO(edda) [**2**], $VO(meox)_2$ [**3**], VO(salen) [**4**], and $[VO(SCN)_4]^{2-}$ [**5**] as a function of the nitrogen ligand type. The solid bars represent $A_{iso}$ values from the ADF (SR UKS, BP86) calculations, and the dotted bars represent the experimentally measured $A_{iso}$.

spin transfer mechanism in which the nitrogen p orbital is polarized by an exchange interaction with the unpaired electron on the vanadium.[56] The SR UKS method includes spin polarization effects and therefore provides very good agreement with experimental data for the nitrogen isotropic hyperfine coupling constant as shown in the bar graph in Figure 2. The spin−orbit contribution to the nitrogen ligand $A_{iso}$ is very small (as expected) and can be assessed by comparing the SO + SR ROKS and the SR ROKS results in Table 1. The only difference between these two calculations is the inclusion of spin−orbit coupling effects in one method but not the other. The results indicate that spin−orbit coupling effects are less than 0.1 MHz.

The anisotropic contributions to the hyperfine coupling constant tensor, $A_{D,x}$, $A_{D,y}$, and $A_{D,z}$, were calculated by three methods, SR UKS, SO + SR ROKS, and SR ROKS, so that the spin polarization and spin−orbit coupling contributions could be evaluated. A comparison of $A_{D,x}$, $A_{D,y}$, and $A_{D,z}$ (SR UKS and SO + SR ROKS) with the experimental values for $A_{D,x}$, $A_{D,y}$, and $A_{D,z}$ can be made by inspection of the data in Table 1. The agreement between $A_{D,x}$, $A_{D,y}$, and $A_{D,z}$ (SR UKS) and the experimental $A_{D,x}$, $A_{D,y}$, and $A_{D,z}$ was very good in comparison with the same values calculated with the SO + SR ROKS method. The SO + SR ROKS and the SR ROKS results were the same within ∼0.1 MHz in almost all cases indicating that spin−orbit coupling contributions to the anisotropic nitrogen hyperfine coupling constant are negligible. Therefore, the best method for calculating the nitrogen $A_D$ value is the SR UKS method although the quantitative agreement is not as good as that for $A_{iso}$ values.

**DFT Calculations of the Nitrogen Quadrupole Coupling Constants for $VO^{2+}$ Model Complexes with Equatorial Amine, Imine, and Isothiocyanate Ligands.** Nitrogen NQCCs can be measured using ESEEM spectroscopy under conditions of *exact cancellation*.[19−23] Exact cancellation for nitrogen nuclei occurs when the nuclear Zeeman interaction and the hyperfine coupling interaction cancel in one-electron spin manifold and pure quadrupole eigenstates remain. Under conditions of exact cancellation, three pure quadrupole peaks are observed in the $^{14}N$ ESEEM spectrum at frequencies of $K(3 + \eta)$, $K(3 - \eta)$, and $2K\eta$, where $K$ is the NQCC, $e^2qQ/4$, and $\eta$ is the asymmetry

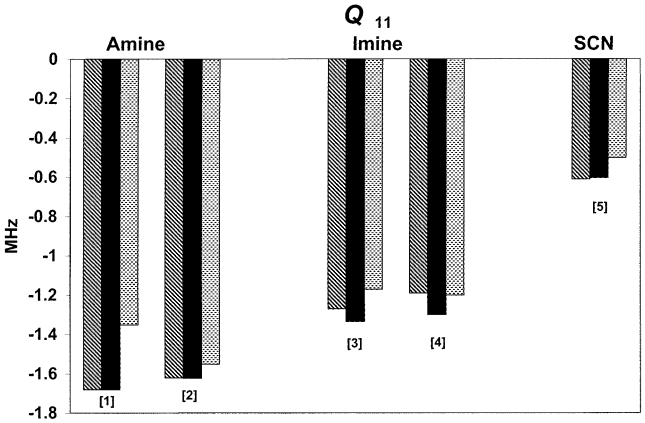


**Figure 3.** The nitrogen quadrupole coupling constant ($Q_{11}$) in MHz for $VO(gly)_2$ [**1**], VO(edda) [**2**], $VO(meox)_2$ [**3**], VO(salen) [**4**], and $[VO(SCN)_4]^{2-}$ [**5**] as a function of the nitrogen ligand type. The solid bars represent $Q_{11}$ values from the SR UKS (ADF, BP86) calculations, the diagonal striped bars represent $Q_{11}$ values from the SO + SR ROKS (ADF, BP86) calculations, and the dotted bars represent the experimentally measured $Q_{11}$.

parameter. The equations for the quadrupole parameters, $Q_{11}$ and $\eta$, are given as follows:

$$Q_{11} = \frac{3e^2qQ}{4I(2I-1)} = \frac{3e^2qQ}{4}$$

$$\eta = \left|\frac{Q_{33} - Q_{22}}{Q_{11}}\right| \qquad (1)$$

where $Q_{11}$, $Q_{22}$, and $Q_{33}$ are the principal values of the traceless quadrupole tensor, $q$ is the field gradient along the principal axis of the largest field gradient ($z$ axis), and $Q$ is the nuclear quadrupole moment.[57] For all of the complexes considered here, $Q_{11}$ lies along (or nearly along) the V−N bond.

The calculated principal values of the nitrogen nuclear quadrupole coupling tensor are listed in Table 1. The computational results for $Q_{11}$ are in good agreement with the experimental data as shown in the bar graph in Figure 3. The solid bars represent $Q_{11}$ values from the SR UKS (ADF, BP86) calculations, the diagonal striped bars represent $Q_{11}$ values from the SO + SR ROKS (ADF, BP86) calculations, and the dotted bars represent the experimentally measured $Q_{11}$. The deviation between the calculated and experimental values ranges from 5% to 25% with an average deviation of 14%. Error bars were not provided for the experimental values, so it is not possible to say whether the agreement is within experimental error. For the amine and isothiocyanate complexes, the results were invariant with respect to the computational methods (SR UKS, SO + SR ROKS, SR ROKS). For the imine complexes, the SO + SR ROKS computational methods provided slightly better accuracy relative to the SR UKS computational method. Qualitatively, the computational results exhibit the same trend as the experimental $Q_{11}$ values in that $Q_{11}$ varies from amine (approximately −1.6 MHz) to imine (approximately −1.2 MHz) to isothiocyanate (approximately −0.65 MHz). Overall, the calculation of the nitrogen NQCC for these complexes was less sensitive to the theoretical method than the nitrogen hyperfine coupling constant calculations. Warncke and co-workers recently reported a DFT computational study of the NQCCs of imidazole derivatives and the impact of the molecular environment.[13] In the study reported here, the effect of the molecular environment has not been investigated but will be incorporated in future work.

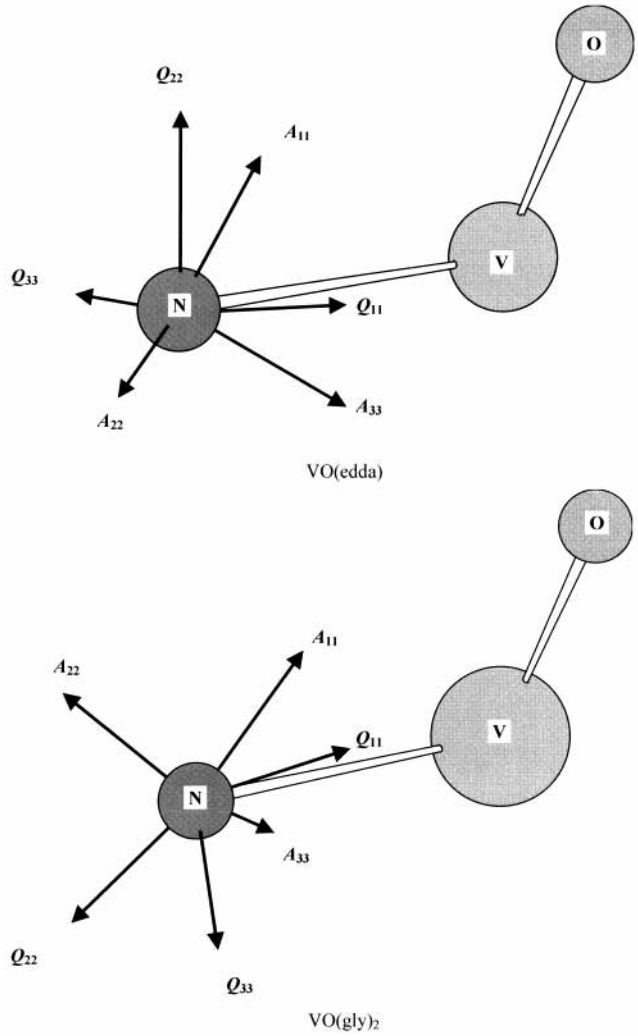


**Figure 4.** Relative orientation of the principal quadrupole and hyperfine axes for the equatorial nitrogen ligands in VO(edda) and $VO(gly)_2$.

**Hyperfine and Quadrupole Principal Axes Orientation.** The DFT calculations also provide the relative orientation of the nitrogen quadrupole and hyperfine tensor axes. The orientations of the nitrogen $A$ and $Q$ tensors from the SR UKS calculations for VO(edda) and $VO(gly)_2$ are shown in Figure 4 in which only the vanadyl nitrogen moiety is shown for clarity. Complete information about the axis orientation for all of the complexes is included in Table S2 as Supporting Information. Experimentally, the orientation of the hyperfine and quadrupole axes is difficult to determine unless single crystal data is available. Therefore, the accuracy of these results is difficult to assess and is subject to some uncertainty, especially given the results of the nitrogen anisotropic hyperfine coupling constant calculations. Further work is needed to address the accuracy of the calculated relative axes orientations. In some cases, a comparison of ESEEM data and simulations gives some information about the relative orientation of the nitrogen quadrupole and hyperfine axis. However, these data are usually qualitative. For example, using ESEEM spectroscopy, Fukui and co-workers determined that the nitrogen quadrupole and hyperfine $Q_{11}$ and $A_{33}$ axes were misaligned for VO(edda) and $VO(gly)_2$.[24] Fukui and co-workers assumed that the $A_{33}$ axis in these complexes corresponded to the V−N bond axis and therefore suggested that the quadrupole axes for these two complexes were deviated relative to the V−N bond. However, the computational results shown in Figure 4 indicate that the

**TABLE 2: Calculated and Experimental Nitrogen Hyperfine and Quadrupole Coupling Constants for $VO^{2+}$ Complexes with Axially Coordinated Ligands[a]**

| | $A_{iso}$ | $A_{D,x}$ | $A_{D,y}$ | $A_{D,z}$ | $Q_{11}$ | $Q_{22}$ | $Q_{33}$ | $\eta$ |
|---|---|---|---|---|---|---|---|---|
| | | | | $VO(H_2O)$ada | | | | |
| SR UKS | −0.10 | −0.29 | −0.20 | 0.49 | −2.52 | 1.38 | 1.14 | 0.09 |
| SO + SR ROKS | 0.55 | −0.33 | −0.21 | 0.54 | −2.50 | 1.36 | 1.14 | 0.09 |
| SR ROKS | 0.56 | −0.34 | −0.22 | 0.56 | −2.50 | 1.36 | 1.14 | 0.09 |
| expt[b] | −1.32 | 0.47 | 0.47 | −0.94 | | | | |
| | | | | $VO(H_2O)$Hheida | | | | |
| SR UKS | −0.63 | −0.26 | −0.21 | 0.47 | −2.40 | 1.24 | 1.16 | 0.03 |
| SO + SR ROKS | 0.01 | −0.26 | −0.35 | 0.61 | −2.39 | 1.24 | 1.16 | 0.03 |
| SR ROKS | 0.02 | −0.27 | −0.36 | 0.63 | −2.39 | 1.24 | 1.16 | 0.03 |
| expt[b] | −1.39 | 0.47 | 0.47 | −0.94 | | | | |

[a] All values in MHz. [b] Reference 6.

quadrupole axes for $VO(gly)_2$ and VO(edda) deviate by only 6° and 8°, respectively, from the V−N bond axis, while the nitrogen hyperfine tensor axes deviate by 45° and 47°, respectively, from the V−N bond axis. Therefore, the computational results can provide guidance for the interpretation of experimental data particularly when assumptions need to be made as in the case above. The computational results for the other complexes in this study suggest a similar trend in that the nitrogen hyperfine tensor axes deviate more from the V−N bond than do the quadrupole tensor axes. However, the deviation of the hyperfine axis relative to the V−N bond is much smaller for the other complexes in this study.

**DFT Calculations of the Nitrogen Hyperfine Coupling Constants for $VO^{2+}$ Model Complexes with Axial Nitrogen Ligands.** Nitrogen ligands coordinated axially to the vanadyl bond are expected to have much smaller ligand hyperfine coupling constants than similar ligands that are equatorially coordinated. The rationalization is that the overlap between the unpaired electron on the vanadium in a $d_{xy}$ orbital and the orbitals of an axial ligand will be very small. Lobrutto and co-workers recently reported ESEEM features attributable to an axially bound nitrogen ligand for model vanadyl aminocarboxylate complexes containing an axial amine ligand.[6] This was the first observation by ESEEM spectroscopy of an axially bound nitrogen ligand. The model complexes that contain ligands that are derivatives of iminodiacetic acid were synthesized and characterized by Hamstra and co-workers.[6] The model complexes each contain a tertiary nitrogen bound trans to the vandyl oxo bond. Using the crystal structures for these complexes (**6** and **7**) shown in Figure 1, the nitrogen hyperfine and quadrupole coupling constants were calculated using the methods discussed earlier. The results are listed in Table 2. The calculated $A_{iso}$ (SR UKS) values are less than 1 MHz, which is qualitatively correct considering the negligible overlap between the ligand orbitals and the unpaired electron in the $d_{xy}$ orbital of vanadium compared to values of 5−7 MHz for equatorial N ligands. Quantitatively, the agreement between experimental and calculated $A_{iso}$ values is quite poor. Because the magnitude of the coupling constants is so small, a small absolute error is a very large percent error.

**Implications for the Interpretation of $^{14}$N ESEEM Spectra.** The computational results reported here indicate that the SR UKS relativistic ZORA method provides excellent qualitative and in some cases quantitative agreement between calculated and experimental nitrogen hyperfine and quadrupole coupling constants for equatorially coordinated ligands in $VO^{2+}$ complexes. The quantitative agreement between the calculated (SR UKS) and experimental $A_{iso}$ for the equatorial nitrogen ligands in all of the complexes was very good (<10%). The quantitative agreement between computational and experimental for the anisotropic $A$ values were generally but not uniformly good. Similarly, the agreement of the calculated and experimental quadrupole coupling constants was generally but not uniformly good. It should be noted that the largest deviations were observed for $VO(gly)_2$, which was also the only complex in this study that was geometry-optimized. Recently, other groups have successfully applied related DFT methods to ligand hyperfine coupling constants for various transition metal complexes.[25−30] Work is in progress in our group to apply these DFT methods to other transition metal complexes to evaluate whether the results reported here will apply to a wider range of transition metal systems.

The molecular environment was not considered in these studies and may contribute to the deviations of the experimental and calculated values. Overall, the effect of the molecular environment is expected to be rather small for the complexes studied here, explaining the good quantitative agreement of experimental and calculated hyperfine coupling constants in many cases. These results suggest that DFT calculations may be very useful for interpreting the ESEEM spectra obtained for vanadoprotein systems. However, the molecular environment may be more important for protein systems and should be incorporated into future computational studies. The computational results for the axial nitrogen ligands were qualitatively correct, but the relative errors were rather large.

## Conclusions

DFT calculations of the EPR parameters for model vanadyl−nitrogen complexes were used to investigate the nitrogen ligand dependence of the nitrogen hyperfine and quadrupole coupling constants. Overall, the DFT calculations confirmed that the nitrogen hyperfine coupling constant varies according to nitrogen ligand type, from amine to imine to isothiocyanate as predicted experimentally by Fukui and co-workers.[24] The agreement between the calculated and experimental nitrogen $A_{iso}$ values for equatorial nitrogen ligands was very good (average deviation of 4%). Equatorial nitrogen nuclear quadrupole coupling constants were also calculated with relatively good accuracy (average deviation of 14%). For axially coordinated nitrogen ligands, the computational results were in qualitative agreement with experiment. The results of this study demonstrate the potential utility of DFT calculations of EPR parameters for interpreting the high-resolution EPR spectra of nitrogen ligands in $VO^{2+}$ complexes.

**Acknowledgment.** S.L. gratefully acknowledges the support of NSF (Grant CHE-02048047) and the University of Iowa (Carver). The calculations were performed on the supercomputer through the National Computational Science Alliance (Grant CHE-020051).

**Supporting Information Available:** The Cartesian coordinates for all of the complexes used in this study (Table S1) and the eigenvectors for the nitrogen $A$ and $Q$ tensors (Table S2). The material is available free of charge via the Internet at http://pubs.acs.org.

## References and Notes

(1) Eaton, S. S.; Eaton, G. R.. In *Vanadium in Biological Systems*; Chasteen, N. D., Ed.; Kluwer Academic Publishers: Dordrecht, Netherlands, 1990; pp 199−222.

(2) Eaton, S. S.; Dubach, J.; More, K., M.; Eaton, G. R.; Thurman, G.; Ambruso, D. R. *J. Biol. Chem.* **1989**, *264*, 4776−4781.

(3) Gerfen, G. J.; Hanna, P. A.; Chasteen, N. D.; Singel, D. J. *J. Am. Chem. Soc.* **1991**, *113*, 9513−9519.

(4) Chasteen, N. D. Vanadium-Protein Interactions. In *Vanadium and its role in life*; Sigel, H., Sigel, A., Eds.; Metal Ions in Biological Systems, Vol. 31; M. Dekker: New York, 1995; pp 231−247.

(5) Chasteen, N. D. Vanadyl(IV) EPR Spin Probes: Inorganic and Biochemical Aspects. In *Biological Magnetic Resonance*; Berliner, L. J., Reuben, J., Eds.; Plenum: New York, 1981; Vol. 3, p 53.

(6) (a) LoBrutto, R.; Hamstra, B. J.; Colpas, G. J.; Pecoraro, V. L.; Frasch, W. D. *J. Am. Chem. Soc.* **1998**, *120*, 4410−4416. (b) Hamstra, B. J.; Houseman, A. L. P.; Colpas, G. J.; Kampf, J. W.; LoBrottu, R.; Frasch, W. D.; Pecoraro, V. *Inorg. Chem.* **1997**, *36*, 4866−4874.

(7) Dikanov, S. A.; Tyryshkin, A. M.; Huttermann, J.; Bogumil, R.; Witzel, H. *J. Am. Chem. Soc.* **1995**, *117*, 4976−4986.

(8) de Boer, E.; Keijzers, C. P.; Reijerse, E. J.; Collison, D.; Garner, C. D.; Wever, R. *FEBS Lett.* **1988**, *235*, 93−97.

(9) Petersen, J.; Hawkes, T. R.; Lowe, D. J. *J. Am. Chem. Soc.* **1998**, *120*, 10978−10979.

(10) Petersen, J.; Hawkes, T. R.; Lowe, D. J. *J. Inorg. Biochem.* **2000**, *80*, 161−168.

(11) Tipton, P. A.; McCracken, J.; Cornelius, J. B.; Peisach, J. *Biochemistry* **1989**, *28*, 5720−5728.

(12) Zhang, C.; Markham, G. D.; LoBrutto, R. *Biochemistry* **1993**, *32*, 9866−9873.

(13) Torrent, M.; Musaev, D. G.; Morokuma, K.; Ke, S. C.; Warncke, K. *J. Phys. Chem. B* **1999**, *103*, 8618−8627.

(14) Oja, T. *Adv. Nucl. Quadrupole Reson.* **1974**, *7*, 401−410.

(15) Marino, R. A. *Adv. Nucl. Quadrupole Reson.* **1974**, *7*, 391−400.

(16) Guibe, L. *Adv. Nucl. Quadrupole Reson.* **1974**, *7*, 375−389.

(17) Flanagan, H. L. S.; David, J. *J. Chem. Phys.* **1987**, *87*, 5606.

(18) Schweiger, A.; Jeschke, G. *Principles of Pulse Electron Paramagnetic Resonance*; Oxford University Press: New York, 2001.

(19) Reijerse, E. J.; Tyryshkin, A. M.; Dikanov, S. A. *Magn. Reson.* **1998**, *131*, 295−309.

(20) Fukui, K.; Ohya-Nishiguchi, H.; Kamada, H. *J. Phys. Chem.* **1993**, *97*, 11858−11860.

(21) Magliozzo, R. S.; Peisach, J. *Biochemistry* **1993**, *32*, 8446−56.

(22) Larsen, S. C.; Singel, D. J. *J. Phys. Chem.* **1992**, *96*, 10594−10597.

(23) Larsen, S. C.; Singel, D. J. *J. Phys. Chem.* **1992**, *96*, 9007−9013.

(24) Fukui, K.; Ohya-Nishiguchi, H.; Kamada, H. *Inorg. Chem.* **1997**, *36*, 5518−5529.

(25) Munzarova, M.; Kaupp, M. *J. Phys. Chem. A* **1999**, *103*, 9966−9983.

(26) Stein, M.; van Lenthe, E.; Baerends, E. J.; Lubitz, W. *J. Phys. Chem. A* **2001**, *105*, 416−425.

(27) Larsen, S. C. *J. Phys. Chem. A* **2001**, *105*, 4563−4573.

(28) Neese, F. *J. Phys. Chem. A.* **2001**, *105*, 4290−4299.

(29) Saladino, A. C.; Larsen, S. C. *J. Phys. Chem. A* **2002**, *106*, 10444.

(30) Hayes, R. G. *Inorg. Chem.* **2000**, *39*, 156−158.

(31) Kanamori, K.; Miyazaki, K.; Okamoto, K. *Acta Crystallogr.* **1997**, *C53*, 672−673.

(32) Shiro, M.; Fernando, Q. *Anal. Chem.* **1971**, *43*, 1222−1230.

(33) Riley, P. E.; Pecoraro, V. L.; Carrano, C. J.; Bonadies, J.; Raymond, K. N. *Inorg. Chem.* **1986**, *25*, 154−160.

(34) Kangjing, Z.; Yuanzhi, X.; Jinling, H. *Jiegou Huaxue* **1984**, *3*, 61−64.

(35) Perdew, J. P. *Phys. Rev. B* **1986**, *33*, 8822−8824.

(36) Becke, A. D. *J. Chem. Phys.* **1993**, *98*, 5648−5652.

(37) Schafer, A.; Huber, C.; Ahlrichs, R. *J. Chem. Phys.* **1994**, *100*, 5829−5835.

(38) Schafer, A.; Horn, H.; Ahlrichs, R. *J. Chem. Phys.* **1992**, *97*, 2571−2577.

(39) Frisch, M. J.; Trucks, G. W.; Schlegel, H. B.; Scuseria, G. E.; Robb, M. A.; Cheeseman, J. R.; Zakrzewski, V. G.; Montgomery, J. A., Jr.; Stratmann, R. E.; Burant, J. C.; Dapprich, S.; Millam, J. M.; Daniels, A. D.; Kudin, K. N.; Strain, M. C.; Farkas, O.; Tomasi, J.; Barone, V.; Cossi, M.; Cammi, R.; Mennucci, B.; Pomelli, C.; Adamo, C.; Clifford, S.; Ochterski, J.; Petersson, G. A.; Ayala, P. Y.; Cui, Q.; Morokuma, K.; Malick, D. K.; Rabuck, A. D.; Raghavachari, K.; Foresman, J. B.; Cioslowski, J.; Ortiz, J. V.; Stefanov, B. B.; Liu, G.; Liashenko, A.; Piskorz, P.; Komaromi, I.; Gomperts, R.; Martin, R. L.; Fox, D. J.; Keith, T.; Al-Laham, M. A.; Peng, C. Y.; Nanayakkara, A.; Gonzalez, C.; Challacombe, M.; Gill, P. M. W.; Johnson, B. G.; Chen, W.; Wong, M. W.; Andres, J. L.; Head-Gordon, M.; Replogle, E. S.; Pople, J. A. *Gaussian 98*, revision A.6; Gaussian, Inc.: Pittsburgh, PA, 1998.

(40) Fonseca Guerra, C.; Snijders, J. G.; Te Velde, G.; Baerends, E. J. *Theor. Chem. Acc.* **1998**, *99*, 391.

(41) Baerends, E. J.; Autschbach, J. A.; Bérces, A.; Bo, C.; Boerrigter, P. M.; Cavallo, L.; Chong, D. P.; Deng, L.; Dickson, R. M.; Ellis, D. E.; Fan, L.; Fischer, T. H.; Fonseca Guerra, C.; van Gisbergen, S. J. A.; Groeneveld, J. A.; Gritsenko, O. V.; Grüning, M.; Harris, F. E.; van den Hoek, P.; Jacobsen, H.; van Kessel, G.; Kootstra, F.; van Lenthe, E.; Osinga, V. P.; Patchkovskii, S.; Philipsen, P. H. T.; Post, D.; Pye, C. C.; Ravenek, W.; Ros, P.; Schipper, P. R. T.; Schreckenbach, G.; Snijders, J. G.; Sola, M.; Swart, M.; Swerhone, D.; Te Velde, G.; Vernooijs, P.; Versluis, L.; Visser, O.; van Wezenbeek, E.; Wiesenekker, G.; Wolff, S. K.; Woo, T. K.; Ziegler, T. *ADF*, 2002.01 ed.; SCM: Amsterdam, The Netherlands, 2002.

(42) Te Velde, G.; Bickelhaupt, F. M.; van Gisbergen, S. J. A.; Fonseca Guerra, C.; Baerends, E. J.; Snijders, J. G.; Ziegler, T. *J. Comput. Chem.* **2001**, 931−967.

(43) van Lenthe, E.; Wormer, P. E. S.; van der Avoird, A. *J. Chem. Phys.* **1997**, *107*, 2488−2498.

(44) van Lenthe, E.; van der Avoird, A.; Wormer, P. E. S. *J. Chem. Phys.* **1998**, *108*, 4783−4796.

(45) van Lenthe, E.; Baerends, E. J.; Snijders, J. G. *J. Chem. Phys.* **1993**, *99*, 4597−4610.

(46) van Lenthe, E.; Baerends, E. J.; Snijders, J. G. *J. Chem. Phys.* **1994**, *101*, 9783−9792.

(47) van Lenthe, E.; Ehlers, A. E.; Baerends, E. J. *J. Chem. Phys.* **1999**, *110*, 8943−8953.

(48) van Lenthe, E.; van Leeuwen, R.; Baerends, E. J.; Snijders, J. G. *Int. J. Quantum Chem.* **1996**, *57*, 281−293.

(49) van Lenthe, E.; Snijders, J. G.; Baerends, E. J. *J. Chem. Phys.* **1996**, *105*, 6505−6516.

(50) Belanzoni, P.; Baerends, E. J.; Gribnau, M. *J. Phys. Chem. A* **1999**, *103*, 3732−3744.

(51) Vosko, S. H.; Wilk, L.; Nusair, M. *Can. J. Phys.* **1980**, *58*, 1200−1211.

(52) Baerends, E. J.; Ellis, D. E.; Ros, P. *Chem. Phys* **1973**, *2*, 41−51.

(53) Te Velde, G.; Baerends, E. J. *J. Comput. Phys.* **1992**, *99*, 84−98.

(54) Versluis, L.; Ziegler, T. *J. Chem. Phys.* **1988**, *88*, 322−328.

(55) Guerra, C. F.; Snijders, J. G.; Te Velde, G.; Baerends, E. J. *Theor. Chem. Acc.* **1998**, *99*, 391−403.

(56) Scholes, C. P.; Falkowski, K. M.; Chen, S.; Bank, J. *J. Am. Chem. Soc.* **1986**, *108*, 1660−1671.

(57) Grant, C. V.; Geiser-Bush, K. M.; Cornman, C. R.; Britt, R. D. *Inorg. Chem.* **1999**, *38*, 6285−6288.